Schulze, M.; Handge, U.A.; Abetz, V.:

Preparation and characterisation of open-celled foams using polystyrene-b-poly(4-vinylpyridine) and poly(4-methylstyrene)-b-poly(4-vinylpyridine) diblock copolymers

In: Polymer (2016) Elsevier

DOI: 10.1016/j.polymer.2016.12.005

Preparation and characterisation of open-celled foams using polystyrene-*b*-poly(4-vinylpyridine) and poly(4-methylstyrene)-*b*-poly(4-vinylpyridine) diblock copolymers

Maria Schulze[1], Ulrich A. Handge[1,*], and Volker Abetz[1,2]

[1] *Helmholtz-Zentrum Geesthacht, Institute of Polymer Research, Max-Planck-Strasse 1, 21502 Geesthacht, Germany*

[2] *University of Hamburg, Institute of Physical Chemistry, Martin-Luther-King-Platz 6, 20146 Hamburg, Germany*

** Ulrich A. Handge (Corresponding author), e-mail: ulrich.handge@hzg.de, phone: +49 4152 87 2446, fax: +49 4152 87 2499*

Abstract

In this study, the potential of amphiphilic diblock copolymers on the example of polystyrene-*b*-poly(4-vinylpyridine) (PS-*b*-P4VP) and poly(4-methylstyrene)-*b*-poly(4-vinylpyridine) (P4mS-*b*-P4VP) for producing open-celled foams was evaluated. The porous foam structure was realised by employing carbon dioxide and water as environmental-friendly blowing agents. Rheological measurements in shear and elongation revealed a similar strain-softening behaviour of the diblock copolymers in the melt state. The transient shear and elongational viscosity of the P4mS homopolymer agreed with the linear viscoelastic prediction. On the contrary, the employed PS homopolymer showed strain-hardening. The rheological behaviour of the PS and P4mS homopolymers is consistent with their foaming ability. The PS homopolymer led to a homogeneous, closed cell structure, while the P4mS homopolymer did not foam at all. Because of strain-softening in melt elongation, the PS-*b*-P4VP diblock copolymer generated homogeneous, open-celled foams throughout the whole sample. In contrast, the P4mS-*b*-P4VP diblock copolymer generated partially open-celled structures in coexistence with compact areas. In this work, it was demonstrated that the combination of carbon dioxide and water led to open-celled diblock copolymer foams even if the major component of the block copolymer generates homogeneous closed-celled foams or is not foamable, respectively.

Keywords: Open-celled polymer foams, diblock copolymers, shear and elongational rheology, WLF equation

1. Introduction

The fabrication of porous polymeric materials is of great interest due to their wide range of applications [1]. Nevertheless, the use of block copolymers for preparing open-celled structures, e.g. polymer foams, is a widely unexplored field in spite of its promising perspectives. Common techniques for the fabrication of porous polymeric materials from block copolymers are the liquid-liquid or the solid-liquid phase separation [2-4]. For these processes, a high amount of organic solvents is required. With the increasing demand of environmental-friendly processing ways, the technique of foaming becomes a suitable alternative for the manufacturing of membranes and open-celled structures [5-8]. Intensive research on open-celled foams is conducted in the field of biodegradable polymers for tissue engineering, e.g., creating porous scaffolds from poly(lactid acid) or foaming of semi-crystalline poly(ε-caprolactone) with subcritical carbon dioxide (CO_2) [9-11]. In the field of membrane technology, Barroso et al. developed anti-fouling membranes of grafted poly(acrylonitrile)-*graft*-poly(ethylene oxide) copolymers by a supercritical CO_2-induced phase inversion method [12, 13]. A blend of poly(methyl methacrylate) and poly(methyl methacrylate)-*co*-poly(butyl acrylate)-*co*-poly(methyl methacrylate) triblock copolymer was foamed with CO_2 to fabricate depth filter and membranes [14]. Thermally induced foaming of polyimide with a high glass transition temperature and a thermally labile poly(caprolactone) yielded high temperature stable and porous polymeric foams by thermal degradation into gaseous components of poly(caprolactone) [15].

Especially amphiphilic diblock copolymers with a hydrophilic and a hydrophobic block are suitable candidates because of the ability to separate into microphases [16-18]. Microphase separation of block copolymers allows the design of open-celled foams where the major component, i.e. the matrix in case of a cylindrical morphology, forms the framework of the cells and the minor component generates the open structure. Xu et al. foamed polyethylene-*b*-poly(ethylene oxide) diblock copolymers with different morphologies and showed that lamellar aligned poly(ethylene oxide) microdomains generated open-celled structures [19]. This type of material can be applied in industrial membrane applications such as water filtration and oil purification [20-22]. The advantage of diblock copolymers is the combination of different properties of both polymers due to the covalent bonding of the two blocks which can lead to, e.g., an enhanced toughness [23, 24]. An additional aspect is the different sorption behaviour of the polymers with respect to applied blowing agents. In this study, the most common blowing agent CO_2 is used because it is environmental-benign and well known for its

plasticisation effect and its reduction of viscosity [25-29]. Previous studies on polystyrene-*b*-poly(4-vinylpyridine) revealed a similar solubility of CO_2 with a weak selectivity towards poly(4-vinylpyridine) [30]. On the contrary, the likewise environmental-friendly blowing agent water is mainly soluble in hydrophilic materials [31, 32]. Hence, the effect of the blowing agent differs within an amphiphilic diblock copolymer and leads to different foaming behaviour and foam structure [33, 34]. Employing two blowing agents can increase the effect of solubility and as a result, generate nanoscopic pores in the foam. This effect was shown by Zhang and Yokohama generating a nanoporous structure in a polystyrene-*b*-poly(2-vinylpyridine) block copolymer, which is similar to the investigated block copolymer in this study, with a mixture of methanol and CO_2 [35].

The foamability of polymers strongly depends on their viscoelastic properties. By conducting rheological measurements of diblock copolymers, the relationship between viscoelastic properties and microscopic properties, such as morphology or molecular architecture, were investigated by several groups [36-38]. Investigations on random and block copolymer melts in order to study elongational viscosities were conducted by Koyama et al. [39]. Only a few works on rheological properties of polystyrene-*b*-poly(4-vinylpyridine) diblock copolymers exist. Matsushita et al. focused their research on determining the viscoelastic properties of polystyrene-*b*-poly(2-vinylpyridine) diblock copolymers [40-42]. The influence of rheological behaviour in extension on the foamability was studied in depth by examining shear and elongational properties of polypropylene [43]. The control of foam structure was examined for polypropylene and long chain branched polypropylene by drawing a relationship between rheological properties and tailoring the polymers with specific morphologies [43]. Studies on polypropylene showed the effect of strain-hardening by blending it with high melt strength, branched polypropylene which led to a decrease of cell size and a smaller fraction of open cells [44]. The same effect was observed when blending polypropylene with nanoclay [45]. An increase in the amount of open cells was obtained by adding cell opener to polyurethane foams whereby the elastic properties and the viscosity declined [46, 47].

This work shows an environmental-friendly technique to fabricate open-celled foams. For this purpose, amphiphilic polystyrene-*b*-poly(4-vinylpyridine) and poly(4-methylstyrene)-*b*-poly(4-vinylpyridine) diblock copolymers are foamed with a mixture of CO_2 and water. The solubility of both blowing agents is investigated as well as the plasticisation effect of CO_2 to exhibit the selective effect of the blowing agents on the diblock copolymers. In addition, rheological studies in shear and elongation allow a correlation between the viscoelastic properties and the foaming behaviour.

Therefore, the influence of the matrix system is discussed. Based on the results of our previous study [30] we focus on diblock copolymers with a number average of the molecular weight close to 200 kg/mol.

2. Experimental section

2.1 Materials

In this work, two diblock copolymers were employed for preparation and investigation of polymer foams: Polystyrene-*block*-poly(4-vinylpyridine) (PS-*b*-P4VP) and poly(4-methylstyrene)-*block*-poly(4-vinylpyridine) (P4mS-*b*-P4VP) diblock copolymers were synthesised via sequential anionic polymerisation (see ref. [30, 48] for synthesis of the PS-*b*-P4VP block copolymer). The polymerisation procedure is schematically shown in Figure 1. First, the polystyrene, respectively the poly(4-methylstyrene) block, was polymerised using *sec*-butyl lithium (*s*-BuLi) as initiator. After finishing this step, 4-vinylpyridine was added to polymerize the second block. The polymerisation was terminated by quenching the solution with methanol. The reaction was carried out in tetrahydrofuran (THF) at -78 °C under purified argon atmosphere. To obtain a polymer powder, the solution was precipitated in water, filtered and finally dried in vacuum.

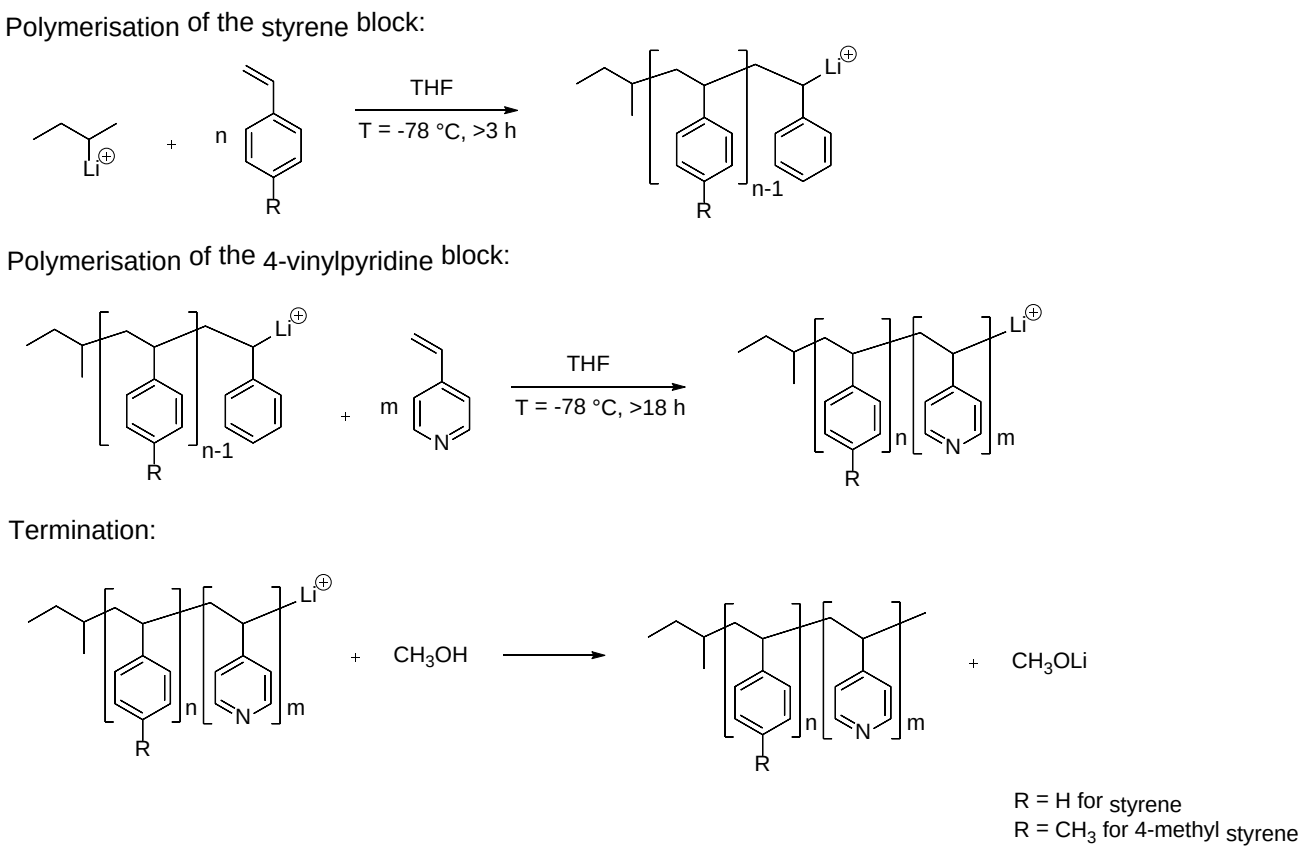

Fig. 1: Synthesis mechanism of the sequential anionic polymerisation of the diblock copolymers of this study.

Polystyrene (PS 158K, BASF SE, Ludwigshafen, Germany), poly(4-methylstyrene) P4mS (P1349-4MeS, Polymer Source Inc., Quebec, Canada) and poly(4-vinylpyridine) P4VP (Sigma Aldrich, München, Germany) were purchased to compare the experimental results of the diblock copolymers with the behaviour of pristine homopolymers.

2.2 **Material characterisation**

The composition of the diblock copolymers was determined by ^{1}H nuclear magnetic resonance spectroscopy (^{1}H-NMR). The measurements were carried out using a Bruker AV-300 FT-NMR spectrometer (Bruker Biospin, Rheinstetten, Germany) at 500 MHz. The diblock copolymer was dissolved in deuterated chloroform ($CDCl_3$) with the internal standard tetramethylsilane (TMS).

Size exclusion chromatography (SEC) was performed to evaluate the number and weight average of the molecular weight (M_n and M_w) of the precursor (polystyrene or poly(4-methylstyrene)), and the

polydispersity ($PDI = M_w/M_n$) of the diblock copolymers. The solvent was dimethylacetamide (DMAc) in the presence of LiCl and the temperature was set to 50 °C. For the measurement, a pre-column and two main columns (PSS Gran 1000 Å 10 µm and PSS Gran 3000 Å 10 µm) were used and a flow rate of 1.0 mL min^{-1} (VWR Hitachi L2130 pump) was applied. The standard for calibration was polystyrene. The molecular weight M_n of the diblock copolymer was calculated using the number average of the molecular weight of the precursors and the evaluated composition of the diblock copolymers based on the ^{1}H-NMR data.

The morphology of the diblock copolymers was investigated by transmission electron microscopy (TEM) using a FEI Tecnai G^2 F20 (FEI, Eindhoven, The Netherlands). Cylindrical samples (preparation see Section 2.4) of the diblock copolymer were cut into approximately 50 nm thick sections with a diamond knife Leica Ultramicrotome EM UCT (Leica Microsystems, Wetzlar, Germany). To contrast the P4VP microdomains, the surface was stained with iodine vapour. The measurement was carried out at a voltage of 120 kV in bright field mode. For analysis of the morphological structure, the P4VP microdomains of the obtained two-dimensional micrographs were evaluated with respect to their diameter using the software Imagic ims Client (Imagic AG, Glattbrugg, Switzerland). To evaluate the experimental results, the Flory-Huggins interaction parameter χ was calculated using the equation:

$$\chi = \frac{V_{0,1-2}}{RT} \cdot A_{1-2} \tag{1}$$

with the averaged segment volume $V_{0,\,1\text{-}2}$, the universal gas constant R, the absolute temperature T and the Hansen solubility parameters difference $A_{1\text{-}2}$ between the polymers [49]. The parameter $A_{1\text{-}2}$ replaces the Hildebrand parameter by including the Hansen solubility parameters with the dispersion (D), polar (P) and hydrogen (H) interaction effects:

$$A_{1-2} = [(\delta_{D2} - \delta_{D1})^2 + 0.25 \cdot (\delta_{P2} - \delta_{P1})^2 + 0.25 \cdot (\delta_{H2} - \delta_{H1})^2] \tag{2}$$

2.3 **Thermal and sorption measurements**

The diblock copolymers were characterised with respect to the thermal stability by thermal gravimetric analysis (TGA). The short-time stability was measured on a TG 209 F1 Iris instrument (Netzsch, Selb, Germany) in a temperature range from 25 °C up to 900 °C and a heating rate of 10 K min^{-1} under argon atmosphere. The long-term stability was evaluated by heating up the sample

to 250 °C with a heating rate of 20 K min^{-1} and holding the temperature for 4 hours before heating up further to 900 °C with the same heating rate of 20 K min^{-1}.

The determination of the glass transition temperature T_g was conducted using a calorimeter DSC 1 (Mettler Toledo, Gießen, Germany). A monoperforated 40 µL aluminum pan was filled with approximately 7 mg of the sample. Then, the sample was heated within a temperature range of 30 °C and 250 °C and a heating rate of 10 K min^{-1} under nitrogen atmosphere to eliminate the thermal history of the sample. After cooling down to 30 °C, the sample was heated up again to 250 °C. This second heating interval was evaluated for the values of T_g.

The influence of the blowing agent CO_2 on the glass transition temperature T_g of the polymers was investigated by high-pressure differential scanning calorimetry (HP-DSC) on a HP-DSC 1 (Mettler Toledo). The sample preparation was similar to the experiments using the conventional DSC except that the lid was multiply perforated to guarantee sufficient gas feed. The measurement parameters were chosen as the ones for conventional DSC, i.e. the heating rate was 10 K min^{-1} and the temperature ranged from 30 °C to 250 °C. First, the sample was heated up to 250 °C and cooled down to 50 °C. Then, CO_2 pressure was applied (1 bar, 10 bar and 20 bar, respectively) and the sample isothermally saturated with CO_2 for 2 h [50]. Last, the sample was heated up to 250 °C under CO_2 pressure but without flow. The saturation time of 2 h was chosen by estimating a theoretical saturation time $t_{sat} \approx R^2/D$ [50] with the assumption of having polymer powder with a single particle size R = 200 µm and a diffusion coefficient $D = 10^{-7}$ cm^2 s^{-1} [30]. Thus, a theoretical saturation time of 1.1 h was calculated which guarantees a complete saturation of the sample after 2 h.

Sorption and diffusion properties were determined using a magnetic suspension balance with a gravimetric sorption analyser IsoSORP® Static (Rubotherm, Bochum, Germany) [51]. Films of the polymers were casted and predried before they were provided in the balance. For complete removal of residues, the samples were evacuated overnight. The measurement was performed at a CO_2 pressure of 40 bar and a temperature of 30 °C. The conditions were set until the mass of the sample achieved a steady state. The diffusion coefficient D was evaluated by fitting the sorption curve using the law of Fickian diffusion:

$$\frac{M_t}{M_\infty} = 4\sqrt{\frac{Dt}{\pi l^2}} \tag{3}$$

with the mass M_t of gas adsorbed in the polymer at time t, the mass M_∞ of gas adsorbed at equilibrium ($t \rightarrow \infty$) and the thickness of the sample l [52]. Equation (3) is an approximation which is valid at short times (i.e. for values $M_t/M_\infty < 0.6$). In order to calculate the saturation time for the employed 2 mm thick samples, the equation $t_{sat} = 0.202\ l^2/D$ [50] is applied with the thickness l of the sample and the experimentally determined diffusion coefficient D.

Besides the sorption behaviour of the blowing agent CO_2, the water uptake was analysed by providing dry samples in a closed glass flask which is filled with ultrapure water and stored in a conditioning cabinet VCL003 (Vötsch Industrietechnik, Reiskirchen-Lindenstruth, Germany) at 30 °C. The samples were weighed in the dry state and then regularly weighed again until the mass reached a steady state.

2.4 **Rheological characterisation in shear and elongation**

All rheological measurements were performed using a rotational rheometer MCR 502 (Anton Paar, Graz, Austria). For the rheological experiments in shear, cylindrical samples with a defined geometry (thickness of 2 mm, diameter of 8 mm) were prepared. Therefore, the dried polymer powder was prepressed at room temperature and then compression-moulded with a pillar press PW 10 H (W/O/Weber, Remshalden, Germany) in the following way: The prepressed polymer tablets were molten under slight pressure for 180 s. Vacuum was applied for 90 s before setting a pressure of approximately 45 kN for 300 s. The temperature was 180 °C. After cooling down the samples, they were stored in a vacuum oven at 40 °C.

The rheological experiments in shear were performed using a plate–plate geometry with a plate diameter of 8 mm. For complete contact between the sample and the plate, the gap was set approximately 0.05 mm smaller than the thickness of the sample. To ensure measurements in the linear viscoelastic regime, first amplitude sweeps were carried out at strain amplitudes γ_0 between 1% and 10% with an angular frequency ω of 10 rad s^{-1}. The subsequent frequency sweeps were conducted under nitrogen atmosphere and constant parameters of strain amplitude γ_0 (5%) and angular frequency range ω (10^{-2} to 10^2 rad s^{-1}) starting with the highest frequency. The temperature of the isothermal experiments was varied between 120 °C and 220 °C in increments of 20 °C. The dynamic moduli were analysed by applying the time-temperature superposition principle using the

software LSSHIFT [53]. The Williams-Landel-Ferry (WLF) equation was applied for analysing the temperature dependence of the shift factor a_T

$$\log a_T = - \frac{c_1(T - T_{ref})}{c_2 + (T - T_{ref})} \quad (4)$$

where c_1 and c_2 are the WLF parameters, T is the measurement temperature and T_{ref} the reference temperature. By fitting eq. (4) to the experimentally measured a_T values, it is possible to determine the WLF parameters c_1 and c_2 and in addition the Vogel temperature T_∞ which is also called "ideal" glass transition temperature [54] and given by $T_\infty = T_{ref} - c_2$.

In addition to the investigation of the rheological properties in shear, rheological experiments in elongation were performed in order to determine the elongational viscosity η_e under uniaxial loading (so-called simple elongation) using a SER-tool (elongational tool SER3/CTD 450, Anton Paar) [55]. Therefore, dried samples with a rectangular geometry (length = 15 mm, width = 10 mm, thickness = 0.8 mm) were compression-moulded and dried at 80 °C in vacuum for minimum 4 h until shortly before the measurements. The temperature was set to 220 °C for the diblock copolymers and to 160 °C for the homopolymers PS and P4mS due to their low viscosity at a temperature of 220 °C. The Hencky strain rate $\dot{\varepsilon}_0$ was 0.01, 0.10 and 1.00 s^{-1} with a maximum Hencky strain ε_{max} of 4. The samples were molten for 4 min with a pre-torque M_{offset} of 10 µNm [56] to avoid sagging during melting. To compare the behaviour in shear and elongation, the transient shear viscosity was multiplied by the Trouton ratio of 3. By applying the software NLREG, a relaxation time spectrum was fitted to the data of the dynamic moduli in order to calculate the linear viscoelastic (LVE) prediction of the elongational viscosity [57, 58]. These theoretical values were compared with the experimentally obtained viscosities in shear and elongation.

2.5 **Foaming of diblock copolymers and characterisation of the cellular structure**

To obtain open porous materials, the diblock copolymers were foamed via the technique of batch foaming. Therefore, cylindrical samples, prepared in the same manner as the tablets for rheology (see Section 2.4), were employed. The foaming process consisted of two steps (see Fig. 2). In the first step, the sample was placed in a high pressure reaction vessel (highpreactor BHM-500, Berghof, Eningen, Germany) which was filled with approximately 250 mL ultrapure H_2O. After closing the vessel carefully, it was filled with CO_2 from a dip-tube bottle (99.995% purity, Linde Gas, Pullingen,

Germany) up to a pressure of 120 bar. The temperature was set to 30 °C and the loading time was 3 days. In the second step, the pressure was released as fast as possible in order to guarantee a sudden pressure drop. Immediately after reaching ambient pressure, the saturated samples were heated up to the foaming temperature which ranged from 110 °C to 200 °C. The pressure drop and the contemporaneous temperature raise initiated the nucleation and the growth of the cells. Finally, the generated foams were vacuum dried.

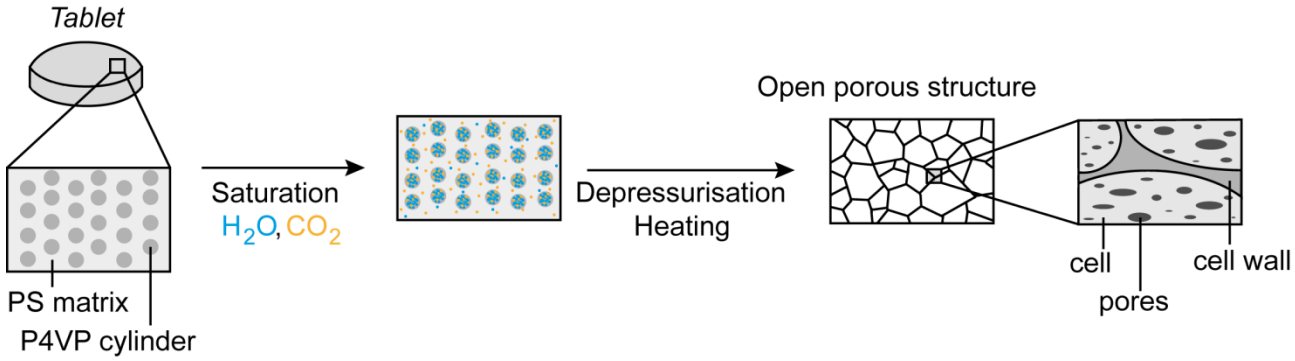

Fig. 2: Experimental approach to generate open porous foams in a two-step batch foaming process.

The foam density was determined using a density determination kit (Mettler Toledo, Greifensee, Switzerland) by applying the Archimedes´ principle. The auxiliary liquid was a perfluoro-compound FC-77 (3M Pharmaceuticals, St. Paul, Minnesota, USA) which was used to calibrate the density shortly before the measurements of the samples.

To obtain information about the cell structure, scanning electron microscopy (SEM) investigations were carried out on a Leo Gemini 1550 VP (Zeiss, Oberkochen, Germany). Therefore, the samples were broken under cryogenic conditions. With a conductive paste (C-Leit, Neubauer Chemikalien, Münster, Germany), the broken foams were attached to the sample holder, and after evaporating of the solvent of the conductive paste, sputtered with a platinum layer of approximately 2 nm thickness. The acceleration voltage varied between 3 kV and 10 kV. If possible, information about the cell size distribution was evaluated with the software Imagic ims Client.

3. Results

3.1 Material characterisation

The molecular characteristics obtained from ^{1}H-NMR and SEC measurements are listed in Table 1. The diblock copolymers are similar in composition and molecular weight in order to ensure comparability of the experimental results with respect to the influence of the chemical structure.

Table 1. Composition and molecular weight of the polymers investigated in this study.

Polymer[a,b]	**PS or P4mS [wt%]**	**P4VP [wt%]**	M_n **[kg mol^{-1}]**	M_w **[kg mol^{-1}]**	***PDI***
PS_{80}-*b*-$P4VP_{20}^{183}$	80	20	183	192	1.07
$P4mS_{81}$-*b*-$P4VP_{19}^{172}$	81	19	172	189	1.10
PS	100	0	113	260	2.30
P4mS	100	0	74	76	1.02
P4VP	0	100	36	61	1.68

[a] Subscript numbers: Fraction of each block in wt%, superscript numbers: weight averaged molecular weight in kg mol^{-1}

[b] Values obtained from SEC measurements using PS standard as reference

To get information about the morphology of the diblock copolymers, transmission electron microscopy was conducted. Figure 3 shows a selected micrograph for each diblock copolymer. Obviously the P4VP microphases of the P4mS-*b*-P4VP diblock copolymer with an average diameter of 71.1 ± 15.1 nm are significantly larger than the P4VP microphases of the PS-*b*-P4VP diblock copolymer with an average diameter of 49.1 ± 7.9 nm. This is due to a stronger segregation of the polymer blocks in the P4mS-*b*-P4VP diblock copolymer indicated by a higher Flory-Huggins interaction parameter χ of 0.90 compared to a χ value of 0.44 for the PS-*b*-P4VP diblock copolymer. It is to be pointed out that different values of the Flory-Huggins interaction parameters are mentioned in the literature [59-62]. The morphology of both materials in the presented micrographs mainly consists of spherical P4VP microdomains in a PS or P4mS matrix without a long-range order. However, one cannot fully exclude that the circles in the micrographs of Figure 3 correspond to cross-sections of cylindrical domains which could be anticipated from Fig. 3(b). Hence we conclude that the composition of these diblock copolymers is located near the spheres-cylinders boundary in the phase diagram.

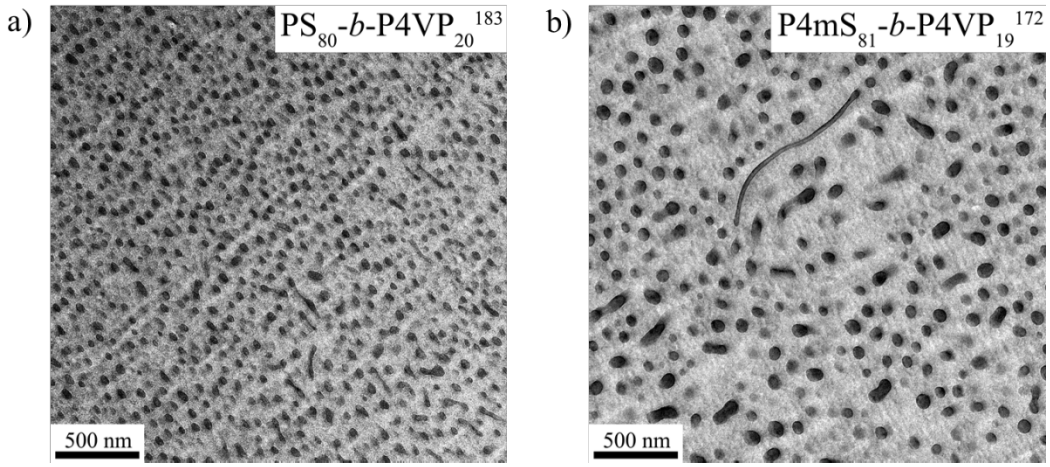

Fig. 3: Transmission electron micrographs of the two diblock copolymers prepared by compression-moulding. In the micrographs, the PS and the P4mS microphases appear bright. The P4VP microphases appear dark.

3.2 **Thermal and sorption measurements**

Thermal gravimetric analysis ensured a thermal stability up to 250 °C for all materials with respect to short- and long-time stability. This knowledge is necessary for selecting the processing parameters for compression-moulding and foaming in order to avoid decomposition of the block copolymer.

Conventional DSC measurements of the glass transition temperatures revealed a value of 104 °C for the PS homopolymer being in the range from 100 °C to 105 °C which is stated in the literature [63, 64]. The T_g for the P4VP homopolymer is determined to be 149 °C similar to literature data [65]. The T_g value of 113 °C of the P4mS homopolymer is higher than stated in the literature, but the conflict in literature data for the T_g of P4mS homopolymers is already mentioned [63] with varying values such as 93 °C [66], 101 °C [67, 68] and 109 °C [69].

The plasticising effect of the blowing agent CO_2 on the polymers is depicted in Fig. 4. The glass transition temperature T_g decreased with increasing CO_2 pressure. All materials showed a reduction of T_g which is at least 10 °C at a CO_2 pressure of 20 bar compared to the conventional measurement in a nitrogen atmosphere at 1 bar. The effect is more pronounced for the homopolymers than for the diblock copolymers. It was not possible to evaluate the T_g for the P4VP microphase of the diblock copolymers due to weak signals at higher CO_2 pressures. Consequently, only the T_g reduction for the PS and the P4mS microphases was analysed. The T_g values of P4mS at all applied pressures were

approximately 10 °C higher than the T_g values of PS. The data of the DSC measurements show that the plasticising effect is roughly similar in these two microphases and leads to the assumption that the solubility of CO_2 in these materials possibly is similar, too. For pristine P4VP, the reduction of T_g is more than 15 °C at a pressure of 20 bar. Hence one can conclude that the plasticising effect of the P4VP block of the diblock copolymers is more pronounced than for the matrix (PS or P4mS, respectively).

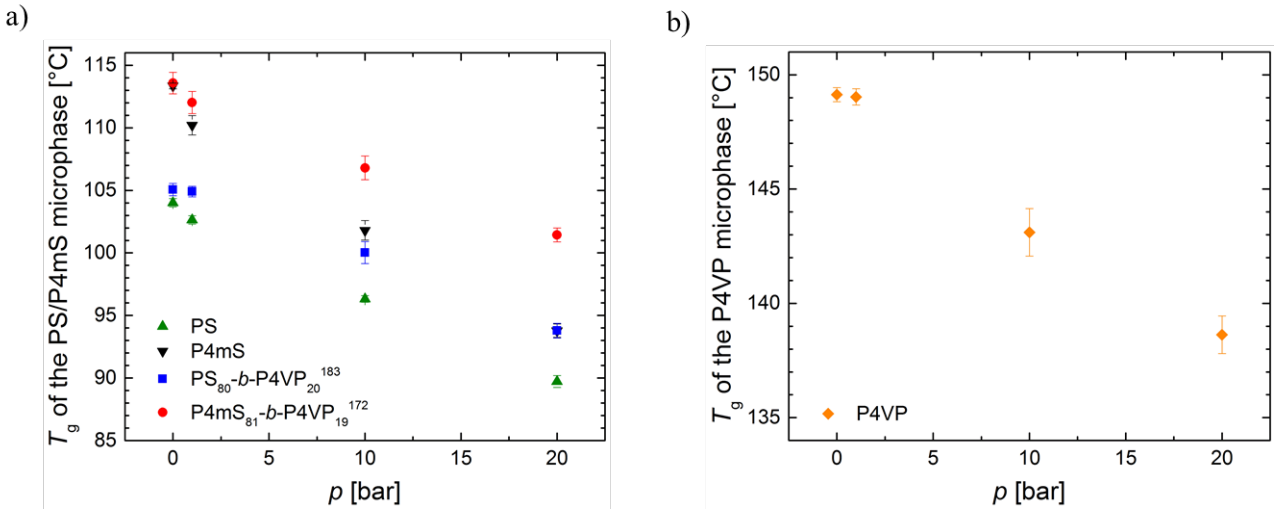

Fig. 4: Plasticising effect of the blowing agent CO_2 shown by a reduction of the glass transition temperature T_g with respect to the applied pressure p in a CO_2 atmosphere for the two diblock copolymers and the three homopolymers.

To analyse the sorption behaviour of the blowing agents, water uptake and specific CO_2-uptake were determined (Table 2). The hydrophobic homopolymers PS and P4mS showed almost no water uptake during the time of measurement whereas the hydrophilic P4VP homopolymer absorbed more than 43 wt% of water. The two diblock copolymers revealed a similar trend with a steady-state value of 2.9 wt% for PS$_{80}$-*b*-P4VP$_{20}^{183}$ and 2.8 wt% for P4mS$_{81}$-*b*-P4VP$_{19}^{172}$. The water uptake of the diblock copolymers did not follow a rule of mixture because the sorption of water into the P4VP microphases is reduced by the PS and P4mS matrix, respectively, which hinders swelling of the P4VP domains. This effect is also visible when comparing the time after the samples reached a water uptake of 90%. The pristine P4VP is 90% saturated after less than 24 h while the diblock copolymers reached this value not until 72 h. However, in spite of the low water sorption of pristine polystyrene, the polystyrene matrix does not completely hinder the diffusion of water into the cylindrical P4VP

domains but slows down diffusion of the water molecules in comparison to pristine P4VP and decreases the overall water-uptake due to limiting swelling of the P4VP domains. By combining CO_2 and water as blowing agents, the CO_2 can enhance the diffusion of the water and swelling of the P4VP domains by plasticising the matrix.

The results for the specific CO_2-uptake did not vary much between the samples. The homopolymers PS and P4mS still showed the lowest CO_2-uptake with 5.9 wt% and 6.2 wt% respectively. The highest CO_2-uptake was obtained by the P4VP homopolymer with a value of 7.2 wt%. Consequently, the values of the two diblock copolymers ranged between the values of the homopolymers: 6.45 wt% for PS_{80}-*b*-$P4VP_{20}^{183}$ and 6.97 wt% for $P4mS_{81}$-*b*-$P4VP_{19}^{172}$. The similar CO_2 solubility of the two diblock copolymers corresponds to the results of the HP-DSC experiments. From the sorption measurements, a strong dependency of the sorption of water and a less pronounced dependency of the sorption of CO_2 with respect to the material can be concluded.

The diffusion coefficient of CO_2 ranges in the same magnitude of order for all materials within experimental scatter. The values vary between $0.43 \cdot 10^{-7}$ cm^2 s^{-1} for P4VP and $0.72 \cdot 10^{-7}$ cm^2 s^{-1} for PS. The diffusion coefficients of the homopolymers correlate with literature data (PS: $0.58 \cdot 10^{-7}$ cm^2 s^{-1} at 25 °C [52], P4VP: $0.13 \cdot 10^{-7}$ cm^2 s^{-1} at 8.25 bar and 35 °C [70]). Using an average diffusion coefficient of $0.50 \cdot 10^{-7}$ cm^2 s^{-1}, the theoretical saturation time was 45 h. The employed saturation time of 72 h guaranteed a complete saturation of CO_2. The information about water uptake, specific CO_2-uptake and the diffusion coefficient of CO_2 is listed in Table 2.

Table 2: Water uptake, specific CO_2-uptake and diffusion coefficient for the two diblock copolymers and the three homopolymers evaluated at a temperature of 30 °C. The sorption measurements were conducted at a pressure of 40 bar.

Polymer	**Water uptake [wt%]**	**Specific CO_2-uptake [wt%]**	**Diffusion coefficient CO_2 [10^{-7} cm^2 s^{-1}]**
PS_{80}-*b*-$P4VP_{20}^{183}$	2.89	6.45	0.45
$P4mS_{81}$-*b*-$P4VP_{19}^{172}$	2.79	6.97	0.44
PS	0.03	5.89	0.72
P4mS	0.08	6.17	0.52
P4VP	43.71	7.18	0.43

3.3 **Rheological properties in shear and elongation**

To investigate the viscoelastic properties of the diblock copolymers, frequency sweeps in the oscillatory mode were conducted at different temperatures and converted into a master curve applying the time-temperature superposition principle. The results were compared with measurements of the homopolymers. The master curves at a reference temperature of 160 °C are presented in Fig. 5.

At high angular frequencies, the PS-*b*-P4VP diblock copolymer behaves similar to polystyrene, but has slightly higher dynamic moduli than pristine PS. At low frequencies a different behaviour compared to PS can be seen (Fig. 5a)). The rubbery plateau is more pronounced for the PS-*b*-P4VP diblock copolymer due to the larger molecular weight of the polystyrene block in comparison to the molecular weight of pristine polystyrene. At lower frequencies, PS clearly shows a terminal regime with the characteristic slopes 2 and 1 for the dynamic moduli G' and G''. On the contrary, the dynamic moduli of the PS-*b*-P4VP diblock copolymer do not depend on frequency at low ω because of the phenomenon of microphase separation. An analogous behaviour is visible for the P4mS-*b*-P4VP diblock copolymer and the P4mS homopolymer (Fig. 5b)). The curves show an almost identical behaviour at high frequencies. However, the rubbery plateau is already considerably broader for the P4mS-*b*-P4VP diblock copolymer than for the P4mS homopolymer because of the larger molecular weight of the P4mS block. The appreciable difference at lower frequencies is again due to microphase separation of the P4mS-*b*-P4VP diblock copolymers and differs from the terminal behaviour of the P4mS homopolymer observable in a decrease of dynamic moduli. The P4VP homopolymer (Fig. 5c)) does not exhibit a distinct rubbery plateau because of the low molecular weight (M_n = 34 kg mol^{-1}) which is close to the entanglement molecular weight. The entanglement molecular weight of P4VP is assumed to be similar to the entanglement molecular weight of PS ($M_{e,PS}$ = 30-40 kg mol^{-1}) [71, 72]. The typical terminal behaviour of the P4VP homopolymer at lower frequencies is clearly seen.

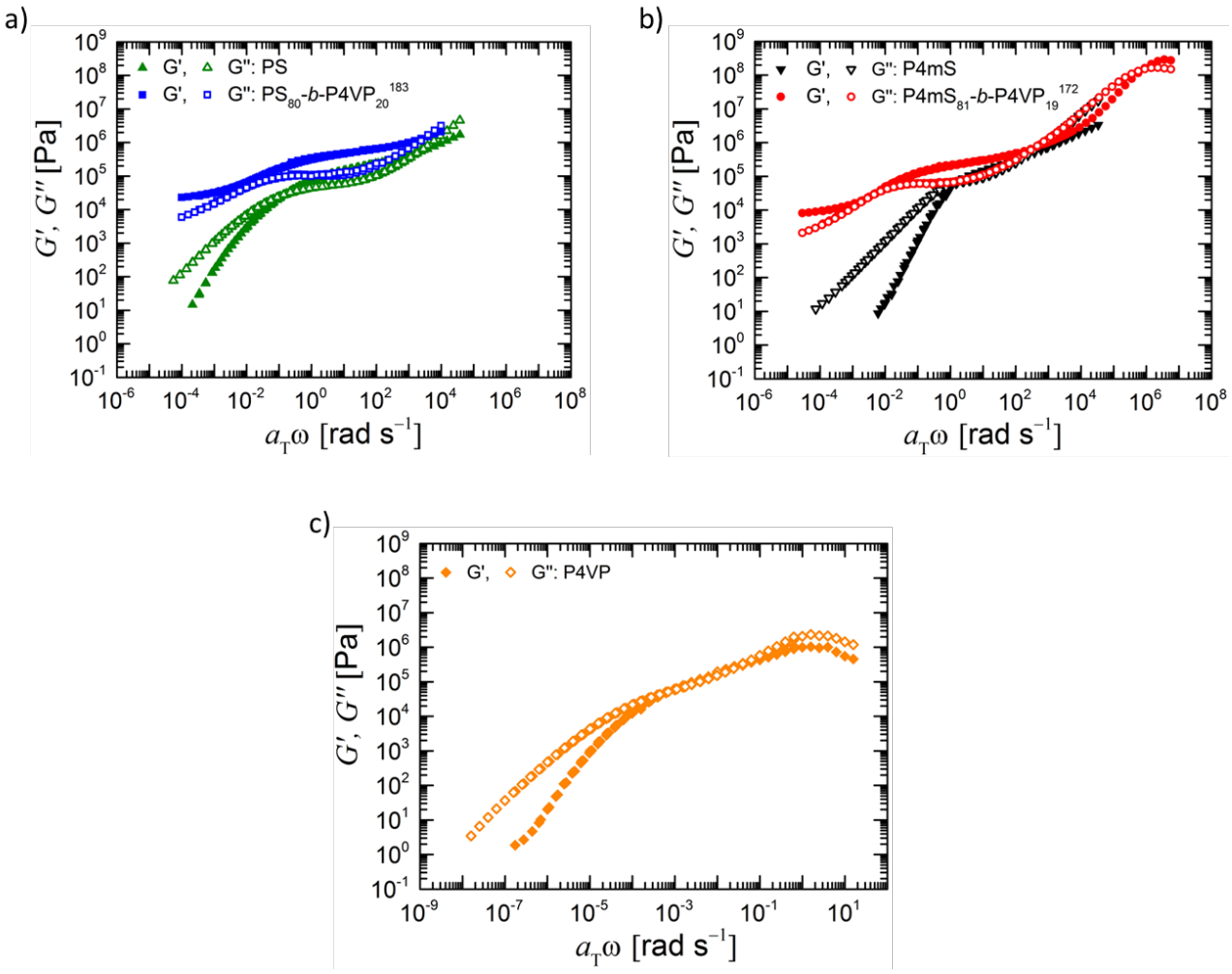

Fig 5: Master curves of the dynamic moduli G' and G'' as a function of the angular frequency ω for a) the PS homopolymer and the PS_{80}-*b*-$P4VP_{20}^{183}$ diblock copolymer, b) the P4mS homopolymer and the $P4mS_{81}$-*b*-$P4VP_{19}^{172}$ diblock copolymer and c) the P4VP homopolymer. The shift factor is denoted by a_T, the strain amplitude γ_0 is 5% and the reference temperature is 160 °C.

Table 3: Zero shear rate viscosity η_0, elastic creep compliance J_e^0 and plateau modulus G_N^0 for the homopolymers and diblock copolymers of this study. Because of microphase separation, no values of zero shear rate viscosity and elastic creep compliance of a Maxwell fluid exist for the two diblock copolymers.

Polymer	**η_0 [Pa s]**	**J_e^0 [Pa^{-1}]**	**G_N^0 [Pa]**
PS_{80}-*b*-$P4VP_{20}^{183}$	-	-	$5.31 \cdot 10^5$
$P4mS_{81}$-*b*-$P4VP_{19}^{172}$	-	-	$2.80 \cdot 10^5$
PS	$1.23 \cdot 10^6$	$1.4 \cdot 10^{-4}$	$1.74 \cdot 10^5$
P4mS	$1.18 \cdot 10^5$	$1.3 \cdot 10^{-5}$	$1.29 \cdot 10^5$
P4VP	$3.65 \cdot 10^8$	$1.5 \cdot 10^{-4}$	$2.75 \cdot 10^5$

By examining the storage modulus at the minimum of tan δ, the plateau modulus G_N^0 can be determined (Table 3). The values of the homopolymers are smaller (P4mS: $1.29 \cdot 10^5$ Pa, PS: $1.74 \cdot 10^5$ Pa, P4VP: $2.75 \cdot 10^5$ Pa) than the values of the diblock copolymers (P4mS-*b*-P4VP: $2.80 \cdot 10^5$ Pa, PS-*b*-P4VP $5.31 \cdot 10^5$ Pa) which is caused by the reinforcement effect of the more rigid P4VP domains. The zero shear rate viscosity η_0 (Table 3) was evaluated for all homopolymers. At a temperature of 160 °C, P4mS has the lowest zero shear rate viscosity of $1.18 \cdot 10^5$ Pa s, followed by PS with $1.23 \cdot 10^6$ Pa s and P4VP with the highest zero shear rate viscosity of $3.65 \cdot 10^8$ Pa s. Since microphase separated diblock copolymers do not behave like a Maxwell fluid, but are associated with a plateau of G' at low frequencies, values of the zero shear rate viscosity of the diblock copolymers in the microphase separated state are not determinable.

The shift factors of the master curves as a function of temperature and the calculated WLF-fit are displayed in Fig. 6 at a reference temperature of 160 °C. Obviously, P4VP has the highest temperature dependency for the homopolymers, since its glass transition temperature does not differ much from 160 °C. On the contrary, PS and P4mS have similar temperature dependencies with P4mS slightly higher than PS. It is clearly seen that the matrix affects mainly the thermal behaviour since the curves of the homopolymers and their corresponding block copolymer are similar. Therefore the WLF parameters of the homopolymer and the related diblock copolymer are similar. The experimental results fit very well to the WLF equation. The parameters c_1 and c_2 of the WLF equation and the Vogel temperature T_∞ are listed in Table 4. Remarkable is the apparent thermorheologically simplicity of microphase separated block copolymers with the ability of

generating master curves and analysing the thermal behaviour with the WLF equation. The reason of the thermorheological simple behaviour is based on the relatively large weight fraction of the matrix component dominating the shift behaviour.

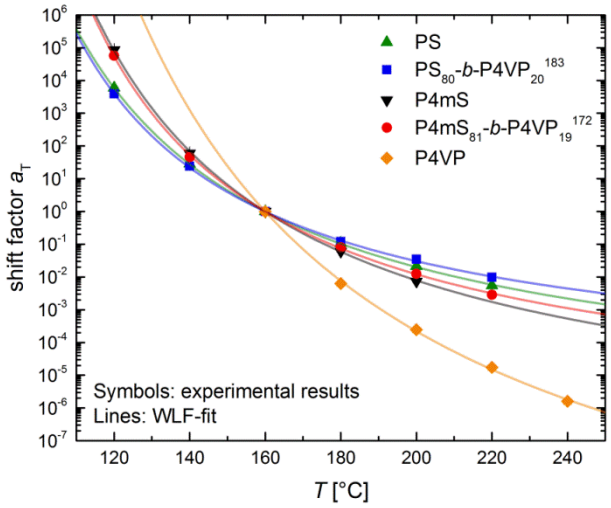

Fig. 6: Shift factor a_T as a function of temperature. The reference temperature is 160 °C. The lines are the result of a fit of the WLF equation to the experimental data.

Table 4: Parameters c_1 and c_2 and Vogel temperature T_∞ obtained from the Williams-Landel-Ferry equation. The reference temperature is 160 °C.

Polymer	c_1	c_2	T_∞ [°C]
PS$_{80}$-*b*-P4VP$_{20}$^{183}	5.2 ± 0.1	98.2 ± 1.9	61.8
P4mS$_{81}$-*b*-P4VP$_{19}$^{172}	6.4 ± 0.1	94.3 ± 1.4	65.7
PS	6.2 ± 0.1	105.2 ± 1.0	54.8
P4mS	7.4 ± 0.2	99.9 ± 2.2	60.1
P4VP	13.4 ± 1.0	106.2 ± 12.0	53.8

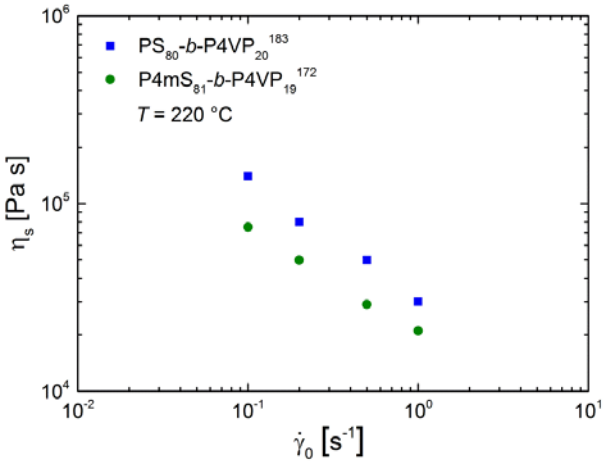

Fig. 7: Steady-state value η_s of the shear viscosity η determined by stress-growth experiments as a function of shear rate $\dot{\gamma}_0$. The test temperature was set to 220 °C.

The steady-state values of the shear viscosity η_s as a function of the shear rate $\dot{\gamma}_0$ are displayed in Fig. 7. The diblock copolymers follow the same trend with a reduction of the shear viscosity when increasing the shear rate. The P4mS-*b*-P4VP diblock copolymer has a lower viscosity than the PS-*b*-P4VP diblock copolymer. The curves indicate a structure-viscous (strain-softening) behaviour.

In polymer foaming, a biaxial elongational flow occurs during cell growth. In order to understand the flow properties in more detail, rheological properties in shear and elongation were compared for the two diblock copolymers (Fig. 8a) and b)) and the two matrix-forming homopolymers PS and P4mS (Fig. 8c) and d)) by plotting the transient elongational viscosity and the shear viscosity which was multiplied by the Trouton ratio of 3. In addition, the linear viscoelastic prediction of the elongational viscosity (LVE) was calculated.

At low times, the experimental data of the transient elongational and shear viscosity are in good agreement for all polymers but the behaviour of the investigated polymers differs strongly at larger times. The PS homopolymer exhibit strain-hardening at larger times which is more pronounced with higher Hencky strain rate, whereas the viscosities of the P4mS homopolymer are independent of the strain rate which is visible by an accordance of elongational and shear viscosities and steady-state values which do not depend on strain rate. At the lowest deformation rate of 0.01 s^{-1} the linear viscoelastic (LVE) prediction of the polystyrene homopolymer agrees with the measured data in the time interval of measurement while the effect of strain-hardening leads to a deviation with increased

Hencky strain rates in melt elongation. For the P4mS homopolymer, the transient elongational and shear viscosity agree to the LVE prediction at all measured deformation rates.

In contrast the PS-*b*-P4VP and P4mS-*b*-P4VP block copolymers show similar rheological properties in shear and melt elongation. Both diblock copolymers show strain-softening at larger times. A dependency of the viscosity on the Hencky strain rate is clearly determinable, while the achievement of a steady-state value is slightly more pronounced for PS-*b*-P4VP compared to P4mS-*b*-P4VP which does not attain a steady-state value in the investigated time interval. The linear viscoelastic prediction does not show a steady-state value due to the plateau of the storage modulus *G'* at low frequencies. An explanation of the strain-softening behaviour is that the shells of the PS and P4ms chains of the block copolymer start sliding on each other which leads to a breakup of the interactions of adjacent P4VP microdomains.

By comparing the block copolymers with the homopolymers, the effect of strain-hardening is not observable for the PS-*b*-P4VP diblock copolymer compared to PS and a dependency on the Hencky strain rate occurs for the P4mS-*b*-P4VP diblock copolymer compared to P4mS. It is assumed, that due to the equivalent behaviour of morphological rearrangements in shear and elongation and similar diffusion and sorption data, the block copolymers show comparable foaming abilities despite the fact that the matrix material behaves very dissimilar.

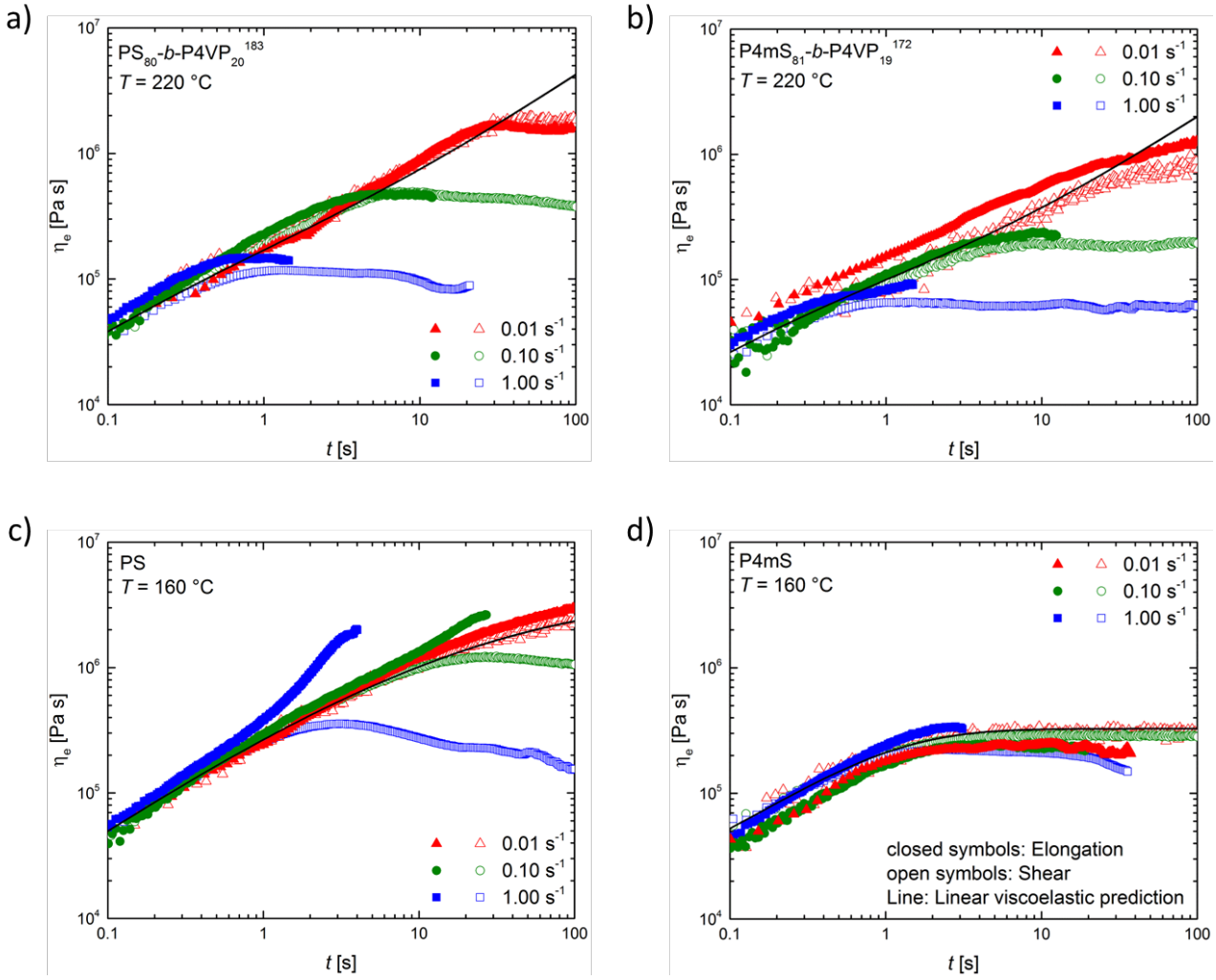

Fig 8: Comparison of the transient elongational viscosity η_e and the shear viscosity (multiplied by the Trouton ratio of 3) as a function of time t for a) PS_{80}-*b*-$P4VP_{20}^{183}$ diblock copolymer, b) $P4mS_{81}$-*b*-$P4VP_{19}^{172}$ diblock copolymer, c) PS homopolymer and d) P4mS homopolymer. Three different Hencky strain rates $\dot{\varepsilon}_0$ were applied. The measurement temperature is indicated. The closed symbols are the data in elongation; the open symbols are the data in shear. The linear viscoelastic prediction of the elongational viscosity (LVE) is also depicted (solid line).

3.4 **Preparation and characterisation of foams**

The foam morphology was investigated using scanning electron microscopy (Fig. 9). Both diblock copolymers show the ability of generating pores in a foam structure in a temperature range between 110 °C and 180 °C when applying the combination of CO_2 and water as blowing agents.

Interestingly, these samples reveal a porous structure in a very small dimension. At higher temperatures, such as 200 °C, the samples were not foamable. Because of the high temperature, the diffusion coefficient of the PS/P4mS matrix was so high that the blowing agents dissolved very rapidly without creating a cellular structure. It is assumable that residuals of the blowing agents stayed in the P4VP microphases and dissolved slower and therefore formed pores while the matrix solidified with a decreasing amount of CO_2 and water. In general, the homogeneity of the foam decreased with increasing foaming temperature for both diblock copolymers. At 110 °C and 150 °C, the sample was foamed completely whereas at 180 °C the samples already exhibited dense areas, and at 200 °C the samples were not foamed anymore. These morphological changes are associated with different values of foam density (Fig. 10). At a foaming temperature of 200 °C, the foam density is close to the bulk density of the block copolymers. A lower foaming temperature yields a smaller foam density. The lowest density of 0.5 g cm^{-3} for PS-*b*-P4VP and of 0.6 g cm^{-3} for P4mS-*b*-P4VP is obtained at a foaming temperature 150 °C. This minimum of foam density at a temperature of 150 °C can be explained by the loss of the blowing agent water which only appears at a temperature above approximately 135 °C as revealed by TGA and DSC data of a PS-*b*-P4VP block copolymer containing water. Further decrease of foaming temperature leads to a higher foam density by a faster solidification of the matrix material.

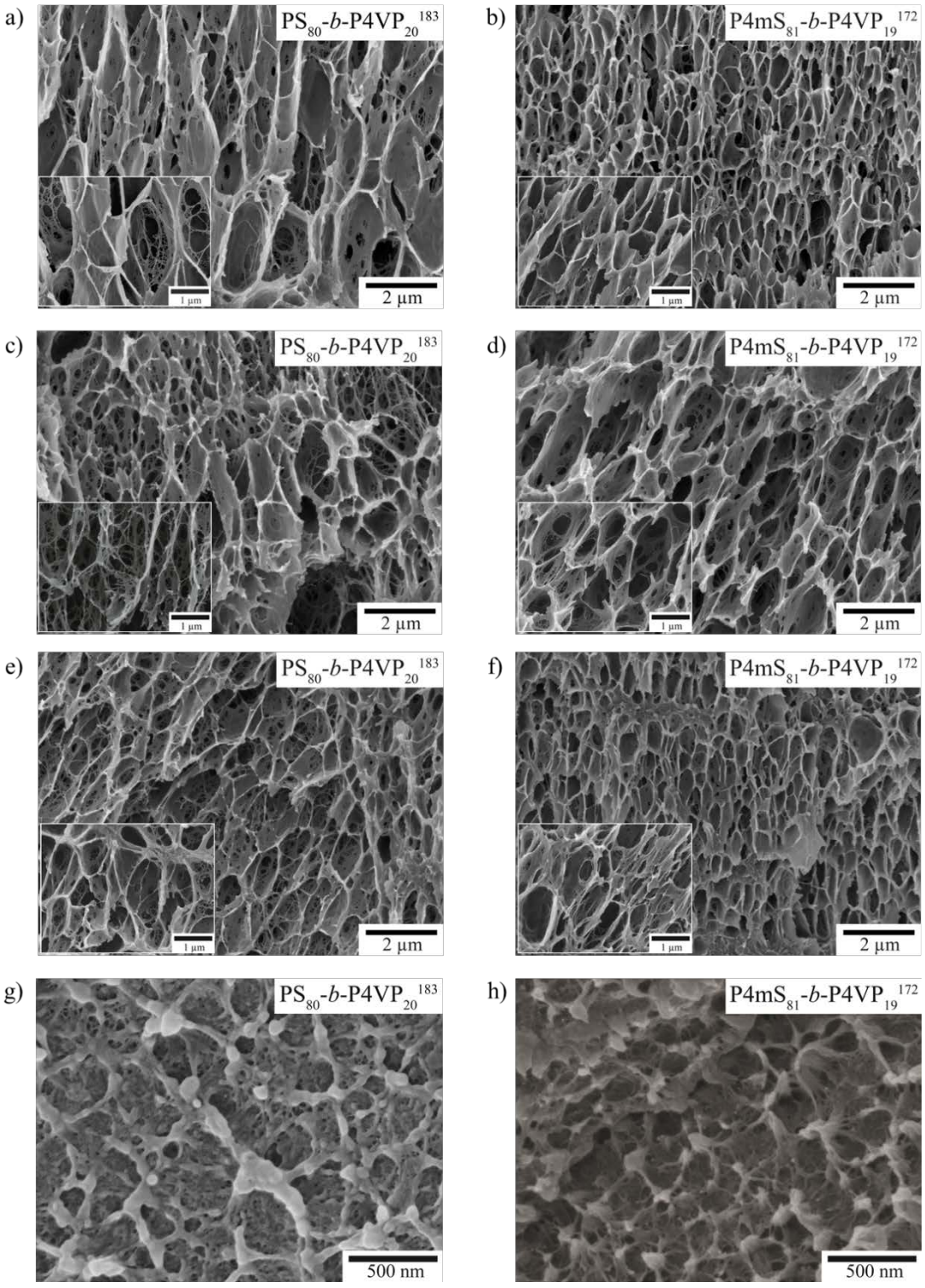

Fig. 9: Scanning electron micrographs showing the foam morphology of PS_{80}-*b*-$P4VP_{20}^{183}$ (left) and $P4mS_{81}$-*b*-$P4VP_{19}^{172}$ (right) diblock copolymers with varying foaming temperatures of a,b) 110 °C, c,d) 150 °C, e,f) 180 °C and g,h) 200 °C.

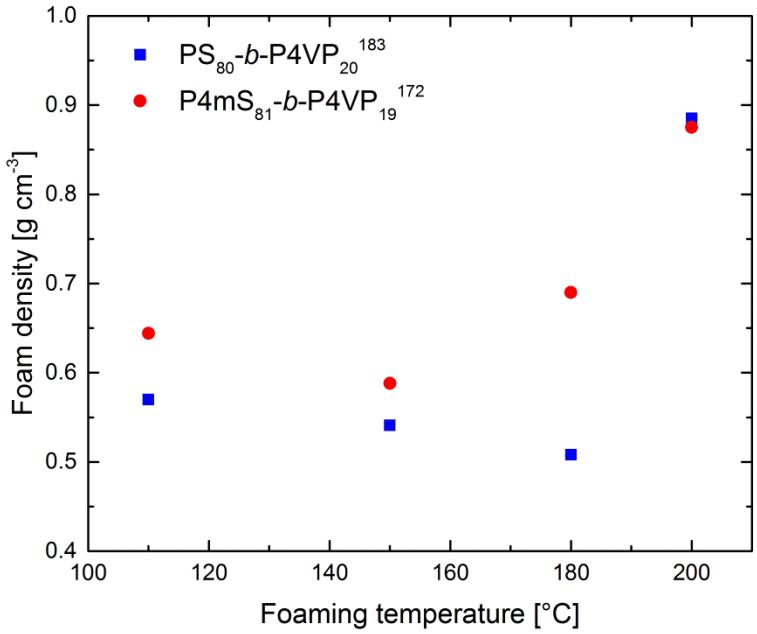

Fig 10: Foam density of the two diblock copolymers with respect to the foaming temperature processed with water and a CO_2-pressure of 120 bar.

The cell size distribution is depicted in Fig. 11. Cells with a diameter smaller than 200 nm were not evaluated due to a limitation of contrasting the obtained micrographs. The mean cell size of PS-*b*-P4VP diblock copolymers is larger than the mean cell size of P4mS-*b*-P4VP diblock copolymers foamed at the same temperature. Both diblock copolymers achieve a maximum cell size at 150 °C which correlates with the lowest density at this temperature. The generation of smaller cell sizes lead to higher densities up to densities close to the bulk material. Almost no foaming was observable at a temperature of 200 °C.

PS-*b*-P4VP diblock copolymers exhibit a broader cell size distribution (i.e. a larger standard deviation) compared to P4mS-*b*-P4VP diblock copolymers. The distribution of cell size of the PS-*b*-P4VP diblock copolymer is generally bell-shaped with a low fraction of smaller cells, a high fraction of mid-sized cells and a low fraction of larger cells whereas the cell size distribution of the P4mS-*b*-P4VP diblock copolymer varies noticeably with foaming temperatures. The foam fabricated at a temperature of 110 °C shows a homogenous distribution with no preferred cell size between 200 nm and 800 nm. On the contrary, the P4mS-*b*-P4VP diblock copolymer foamed at 150 °C reveal a low fraction of small cells, the highest fraction (ca. 18% of all cells) with a cell size between 600 and 700 nm and a relatively high amount of cells larger than 1200 nm. Approximately 50% of the cells of

the P4mS-*b*-P4VP diblock copolymer foamed at 180 °C are smaller than 400 nm. The maximum cell size is approximately 900 nm with an amount of less than 1%.

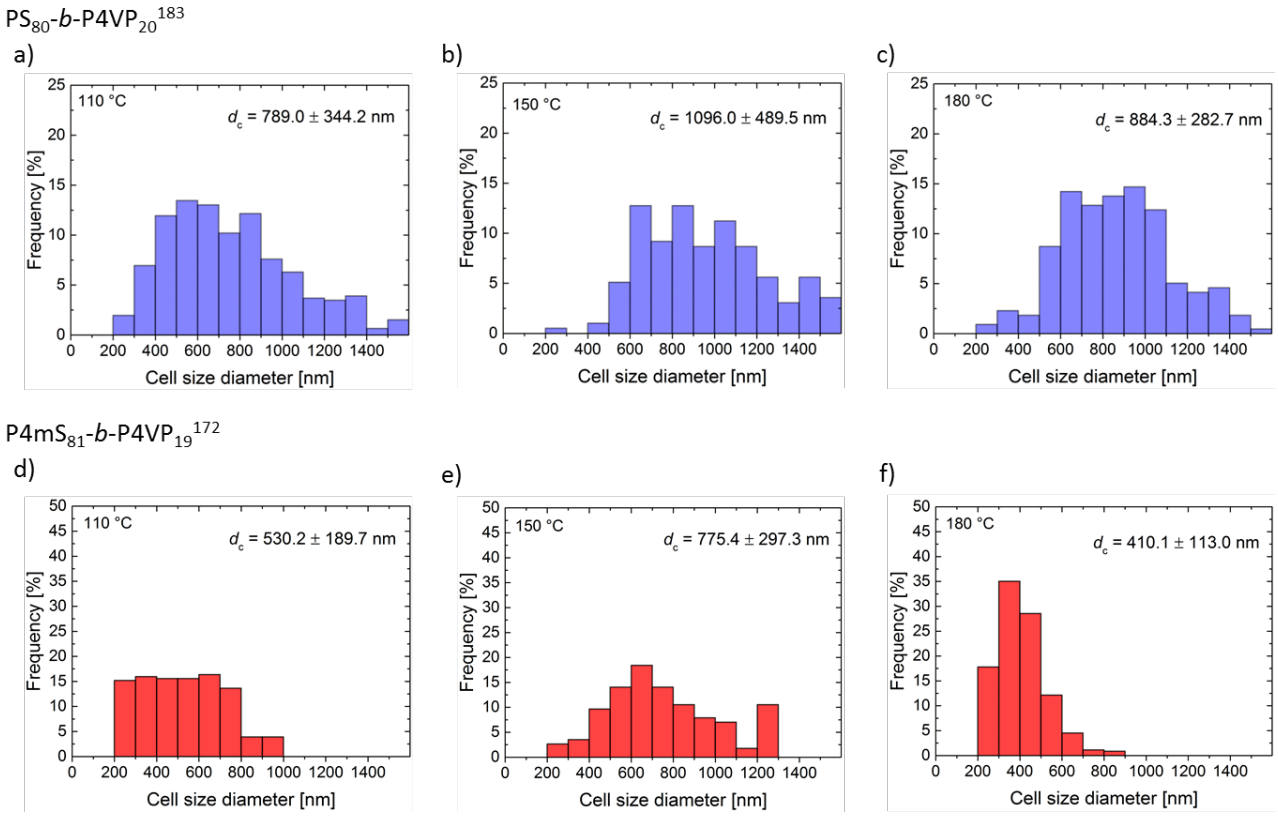

Fig. 11: Cell size distribution of a-c) PS_{80}-*b*-$P4VP_{20}^{183}$ and d-f) $P4mS_{81}$-*b*-$P4VP_{19}^{172}$ diblock copolymers foamed at a, d) 110 °C, b, e) 150 °C and c, f) 180 °C. The average diameter d_c of the cell size is indicated.

Based on the fact that the diblock copolymers resemble each other with respect to their rheological properties, the foaming ability are very alike as well as assumed before. Nevertheless, the obtained foams of the P4mS-*b*-P4VP diblock copolymer show a less homogeneous structure than the PS-*b*-P4VP diblock copolymer (Fig. 12 a)-b)). One reason may be the foaming ability of the matrix system. Figure 12 compares the foams of the diblock copolymers with the foams of the homopolymers. Polystyrene is highly foamable and generates a homogeneous cellular structure. The phenomenon of strain-hardening stabilises the cells during cell growth and prevents their rupture leading to a closed-cell foam. Because of strain-softening in melt extension, the foams of the two diblock copolymers are associated with an open-celled structure. The foams of its PS-*b*-P4VP diblock copolymers are not as

homogeneous as the homopolymer but the foam structure consists of uniformly distributed open foam cells over the whole sample. However, the cell diameter is considerably smaller in the block copolymer than in the homopolymer. Due to the P4VP block with a higher T_g, the expansion of the cells is finished faster by a freezing of this minor component. In contrast, P4mS does not generate a foam structure under the present conditions. The blowing agent diffuses immediately out of the polymer without creating cells which additionally could not be stabilised by the soft matrix. Interestingly, the P4mS-*b*-P4VP diblock copolymer has the ability to develop an open-celled foam structure. By adding a P4VP block, the cells are stabilised due to the more glassy properties of the P4VP block. However, the foaming behaviour of P4mS leads to inhomogeneous foams with high density areas for the P4mS-*b*-P4VP diblock copolymer.

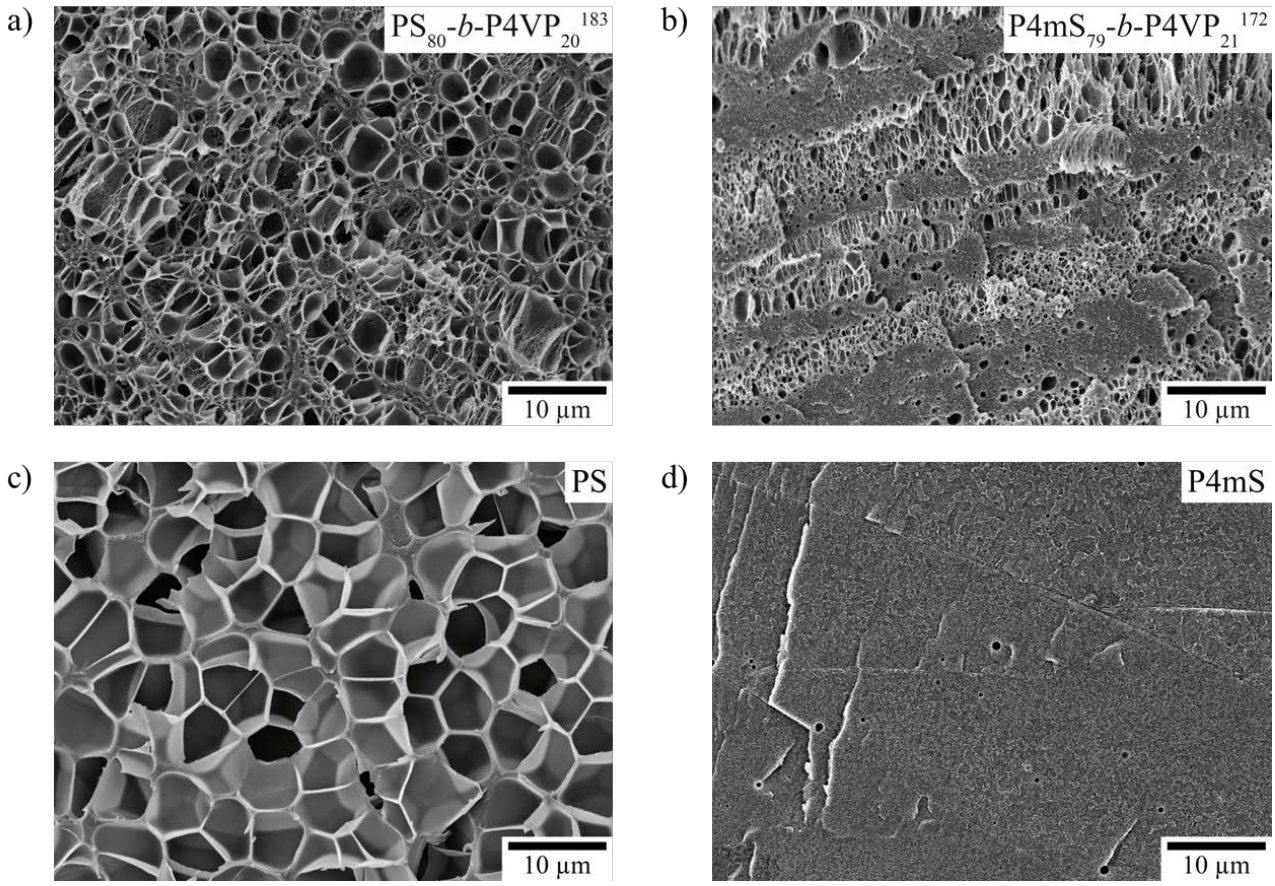

Fig. 12: Foams of a) PS-*b*-P4VP, b) P4mS-*b*-P4VP diblock copolymers, c) PS and d) P4mS homopolymers. The foaming conditions were identical with a pressure of 120 bar and a foaming temperature of 150 °C.

4. Conclusions

This work presents an environmental-friendly way to fabricate open-celled foams by introducing amphiphilic diblock copolymers of PS-*b*-P4VP and P4mS-*b*-P4VP. These diblock copolymers were synthesised via sequential anionic polymerisation which allowed tailoring the molecular weight and composition in order to obtain comparable diblock copolymers. The amphiphilic character with its microphase separation was confirmed by rheological measurements in oscillatory shear and by transmission electron microscopy.

The open-celled structure was achieved by batch foaming with CO_2 and water as the blowing agents. It was shown that the two diblock copolymers absorbed similar amounts of CO_2 (approx. 6 wt%) compared to the homopolymers whereas the water-uptake differed strongly with the kind of polymer. PS and P4mS absorbed less than 1 wt% of water compared to almost 44 wt% of water-uptake for P4VP. The low amount of water-uptake for the diblock copolymers (<3 wt%) is based on the severe diffusion through the PS or P4mS matrix and the hindering of swelling of the P4VP microdomains in the PS or P4mS matrix, respectively, which can be increased by the plasticisation effect of the CO_2 on the matrix. This effect was shown by conducting high-pressure DSC experiments where a reduction of T_g of more than 10 °C (at 20 bar CO_2 pressure) was observable. Rheological measurements revealed an analogous behaviour in shear and elongation for different Hencky strain rates. The two diblock copolymers exhibited strain-softening. In contrast, for the PS homopolymer the effect of strain-hardening was observable, and the P4mS homopolymer behaved in agreement with its linear viscoelastic prediction. After foaming, the PS homopolymer formed very homogenous cells with a closed-cell structure. On the contrary, the P4mS homopolymer did not foam. The diblock copolymers showed coherent rheological properties in shear and elongation as well as coherent foaming behaviour with similar cell structures. However, the foams of PS-*b*-P4VP revealed all over the sample an open-celled structure whereas in the foams of P4mS-*b*-P4VP also dense areas were formed.

Acknowledgment

The authors thank Brigitte Lademann for the synthesis of the diblock copolymers. They acknowledge the experimental support of Clarissa Abetz and Anke-Lisa Metze (transmission and scanning electron microscopy), Silvio Neumann (nuclear magnetic resonance spectroscopy), Maren

Brinkmann (size exclusion chromatography), Jelena Lillepärg (sorption measurements) and Ivonne Ternes (thermal analysis and rheological measurements).

References

[1] Berro S, El Ahdab R, Hassan HH, Khachfe H, and Hajj-Hassan A. Journal of Nanomaterials 2015:21.
[2] Peinemann K-V, Abetz V, and Simon PFW. Nat Mater 2007;6(12):992-996.
[3] Lloyd DR, Kim SS, and Kinzer KE. Journal of Membrane Science 1991;64(1–2):1-11.
[4] Wang YQ, Noga DE, Yoon K, Wojtowicz AM, Lin ASP, Garcia AJ, Collard DM, and Weck M. Advanced Functional Materials 2008;18(22):3638-3644.
[5] Abetz V. Macromolecular Rapid Communications 2015;36(1):10-22.
[6] Krause B, Diekmann K, van der Vegt NFA, and Wessling M. Macromolecules 2002;35(5):1738-1745.
[7] Jacobs LJM, Kemmere MF, and Keurentjes JTF. Green Chemistry 2008;10(7):731-738.
[8] Sauceau M, Fages J, Common A, Nikitine C, and Rodier E. Progress in Polymer Science 2011;36(6):749-766.
[9] Tai H, Popov VK, Shakesheff KM, and Howdle SM. Biochemical Society Transactions 2007;35:516-521.
[10] Nawaby AV, Farah AA, Liao X, Pietro WJ, and Day M. Biomacromolecules 2005;6(5):2458-2461.
[11] Bhamidipati M, Scurto AM, and Detamore MS. Tissue Engineering Part B-Reviews 2013;19(3):221-232.
[12] Barroso T, Temtem M, Casimiro T, and Aguiar-Ricardo A. The Journal of Supercritical Fluids 2011;56(3):312-321.
[13] Zhang A, Zhang Q, Bai H, Li L, and Li J. Chemical Society Reviews 2014;43(20):6938-6953.
[14] Pinto J, Dumon M, Rodriguez-Perez MA, Garcia R, and Dietz C. The Journal of Physical Chemistry C 2014;118(9):4656-4663.
[15] Hedrick JL, Carter KR, Richter R, Miller RD, Russell TP, Flores V, Meccereyes D, Dubois P, and Jérôme R. Chemistry of Materials 1998;10(1):39-49.
[16] Abetz V and Simon PFW. Phase Behaviour and Morphologies of Block Copolymers. Block copolymers I, vol. 189: Springer, 2005. pp. 125-212.
[17] Bates FS and Fredrickson GH. Physics Today 1999;52(2):32.
[18] Abetz V and Boschetti-de-Fierro A. 7.02 - Block Copolymers in the Condensed State. In: Möller KM, editor. Polymer Science: A Comprehensive Reference. Amsterdam: Elsevier, 2012. pp. 3-44.
[19] Xu Y, Liu T, Yuan W-k, and Zhao L. Industrial & Engineering Chemistry Research 2015;54(28):7113-7121.
[20] Shimizu T, Koshiro S, Yamada Y, and Tada K. Journal of Applied Polymer Science 1997;65(1):179-186.
[21] Darder M, Aranda P, Luisa Ferrer M, Gutierrez MC, del Monte F, and Ruiz-Hitzky E. Advanced Materials 2011;23(44):5262-5267.
[22] Yuan Z-Y and Su B-L. Journal of Materials Chemistry 2006;16(7):663-677.
[23] Ruckdäschel H, Altstädt V, and Müller AHE. Cellular Polymers 2007;26(6):367-380.
[24] Macosko CW, Jeon HK, and Hoye TR. Progress in Polymer Science 2005;30(8–9):939-947.
[25] Alessi P, Cortesi A, Kikic I, and Vecchione F. Journal of Applied Polymer Science 2003;88(9):2189-2193.
[26] Shieh Y-T, Su J-H, Manivannan G, Lee PHC, Sawan SP, and Dale Spall W. Journal of Applied Polymer Science 1996;59(4):707-717.
[27] Huang E, Liao X, Zhao C, Park CB, Yang Q, and Li G. ACS Sustainable Chemistry & Engineering 2016;4(3):1810-1818.
[28] Royer JR, Gay YJ, Desimone JM, and Khan SA. Journal of Polymer Science Part B: Polymer Physics 2000;38(23):3168-3180.
[29] Park HE and Dealy JM. Macromolecules 2006;39(16):5438-5452.
[30] Schulze M, Handge UA, Rangou S, Lillepärg J, and Abetz V. Polymer 2015;70(1):88-99.
[31] Yeh S-K, Yang J, Chiou N-R, Daniel T, and Lee LJ. Polymer Engineering & Science 2010;50(8):1577-1584.
[32] Boissard CIR, Bourban P-E, Tingaut P, Zimmermann T, and Månson J-AE. Journal of Reinforced Plastics and Composites 2011;30(8):709-719.
[33] Shinkai T, Ito M, Sugiyama K, Ito K, and Yokoyama H. Soft Matter 2012;8(21):5811-5817.
[34] Yokoyama H and Sugiyama K. Macromolecules 2005;38(25):10516-10522.
[35] Zhang R and Yokoyama H. Macromolecules 2009;42(10):3559-3564.
[36] Gil Haenelt T, Georgopanos P, Abetz C, Rangou S, Alisch D, Meyer A, Handge UA, and Abetz V. Korea-Australia Rheology Journal 2014;26(3):263-275.
[37] Chakkalakal GL, Abetz C, Vainio U, Handge UA, and Abetz V. Polymer 2013;54(15):3860-3873.
[38] Han CD, Baek DM, Kim JK, and Chu SG. Polymer 1992;33(2):294-305.
[39] Takahashi T, Takimoto J, and Koyama K. Journal of Applied Polymer Science 1998;69(9):1765-1774.
[40] Takahashi Y, Ochiai N, Matsushita Y, and Noda I. Polymer Journal 1996;28(12):1065-1070.

[41] Fang L, Takahashi Y, Takano A, and Matsushita Y. Nihon Reoroji Gakkaishi 2013;41(2):93-99.
[42] Fang L, Takahashi Y, Takano A, and Matsushita Y. Macromolecules 2013;46(17):7097-7105.
[43] Xu Z, Zhang Z, Guan Y, Wei D, and Zheng A. Journal of Cellular Plastics 2013;49(4):317-334.
[44] Laguna-Gutierrez E, Van Hooghten R, Moldenaers P, and Rodriguez-Perez MA. Journal of Applied Polymer Science 2015;132(33):14.
[45] Chaudhary AK and Jayaraman K. Polymer Engineering & Science 2011;51(9):1749-1756.
[46] Song KC, Lee SM, and Lee DH. Polymer-Korea 2001;25(5):679-690.
[47] Song KC, Lee SM, and Lee DH. Polymer-Korea 2002;26(2):218-226.
[48] Rangou S, Buhr K, Filiz V, Clodt JI, Lademann B, Hahn J, Jung A, and Abetz V. Journal of Membrane Science 2014;451:266-275.
[49] Hansen CM. Hansen Solubility Parameters: A User's Handbook, 2 ed. Boca Raton: CRC Press 2007.
[50] Handge UA and Altstädt V. Journal of Rheology 2012;56(4):743-766.
[51] Sato Y, Takikawa T, Takishima S, and Masuoka H. Journal of Supercritical Fluids 2001;19(2):187-198.
[52] Crank J and Park GS. Diffusion in Polymers Academic Press, New York 1968.
[53] Honerkamp J and Weese J. Rheologica Acta 1993;32(1):57-64.
[54] Kipnusu WK, Elmahdy MM, Tress M, Fuchs M, Mapesa EU, Smilgies D-M, Zhang J, Papadakis CM, and Kremer F. Macromolecules 2013;46(24):9729-9737.
[55] Hachmann P and Meissner J. Journal of Rheology 2003;47(4):989-1010.
[56] Aho J, Rolón-Garrido V, Syrjälä S, and Wagner M. Rheologica Acta 2010;49(4):359-370.
[57] Freiburg. Materials Research Center, Service group scientific data processing, NLREG (non-linear-regularization), Software Version May 2008.
[58] Honerkamp J and Weese J. Rheologica Acta 1993;32(1):65-73.
[59] Alberda van Ekenstein GOR, Meyboom R, ten Brinke G, and Ikkala O. Macromolecules 2000;33(10):3752-3756.
[60] Chang LL and Woo EM. Polymer 2003;44(5):1711-1719.
[61] Han SH, Lee DH, and Kim JK. Macromolecules 2007;40(20):7416-7419.
[62] Zha W, Han CD, Lee DH, Han SH, Kim JK, Kang JH, and Park C. Macromolecules 2007;40(6):2109-2119.
[63] Brandrup J, Immergut EH, Grulke EA, Abe A, and Bloch DR. Polymer handbook: Wiley New York etc, 1989.
[64] Rieger J. Journal of Thermal Analysis and Calorimetry 1996;46(3-4):965-972.
[65] Shibata M, Kimura Y, and Yaginuma D. Polymer 2004;45(22):7571-7577.
[66] Dunham K, Faber J, Vandenberghe J, and Fowler W. Journal of Applied Polymer Science 1963;7(3):897-908.
[67] Gao H and Harmon JP. Thermochimica acta 1996;284(1):85-102.
[68] Corrado L. The Journal of Chemical Physics 1969;50(5):2260-2262.
[69] Brunacci A, Cowie JMG, Ferguson R, Gómez Ribelles JL, and Vidaurre Garayo A. Macromolecules 1996;29(24):7976-7988.
[70] Shieh JJ and Chung TS. Journal of Polymer Science Part B: Polymer Physics 1999;37(20):2851-2861.
[71] Vapaavuori J, Ras RHA, Kaivola M, Bazuin CG, and Priimagi A. Journal of Materials Chemistry C 2015;3(42):11011-11016.
[72] Wang X, Pellerin C, and Bazuin CG. Macromolecules 2016;49(3):891-899.